J. Fluid Mech. (1974), *vol.* 66, *part* 4, *pp.* 673–687
Printed in Great Britain

The pressure field due to a large circular capped air bubble rising in water

By G. M. LAZAREK† AND H. LITTMAN

Fluid Chemical and Thermal Processes Division, Rensselaer Polytechnic Institute, Troy, New York, 12181

(Received 25 June 1973 and in revised form 13 June 1974)

The pressure field due to a large circular capped air bubble rising in water has been determined experimentally. The results verify the Davies & Taylor cap boundary condition and the frontal pressure field is well approximated by that due to irrotational flow around an oval body.

The pressure field extends axially as far as ten bubble half-widths below the bubble floor. Immediately below the floor the pressure is constant for about two-thirds of a bubble height. The wake is closed and contains symmetric pressure minima. For the bubbles studied, turbulence, as well as the diffusion of vorticity, probably controls the momentum distribution and energy dissipation in the wake.

1. Introduction

Past investigations of spherical and circular capped bubbles have dealt primarily with determining the bubble's shape and rate of rise. As a result of this research, a number of methods are available for accurately predicting the rise velocity of a spherical or circular capped bubble (Collins 1965*a*; Davies & Taylor 1950; Haberman & Morton 1953; Maneri & Mendelson 1968; Mendelson 1967; Rosenberg 1950). The bubble shape in terms of its angular half-width or height-to-width ratio can also be determined (Collins 1965*b*; Davies & Taylor 1950; Grace & Harrison 1967). Recently, a more fundamental understanding of the fluid motion surrounding the bubble has become of interest and has led to flow visualization studies of the bubble's wake structure (Collins 1965*c*; Crabtree & Bridgwater 1967; Maxworthy 1967). These studies have been instrumental in yielding qualitative information about the flow field by indicating possible areas or zones where the fluid motion may be treated as irrotational and where more complicated effects such as turbulence and viscous shear may be important.

In this paper detailed measurements of the entire pressure field around a circular capped air bubble are presented. The measurements are used to verify the Davies & Taylor boundary condition and to develop a realistic analytical model for the region of flow in front of a two-dimensional bubble rising at its

† Present address: Knolls Atomic Power Laboratory, General Electric Company, Schenectady, New York.

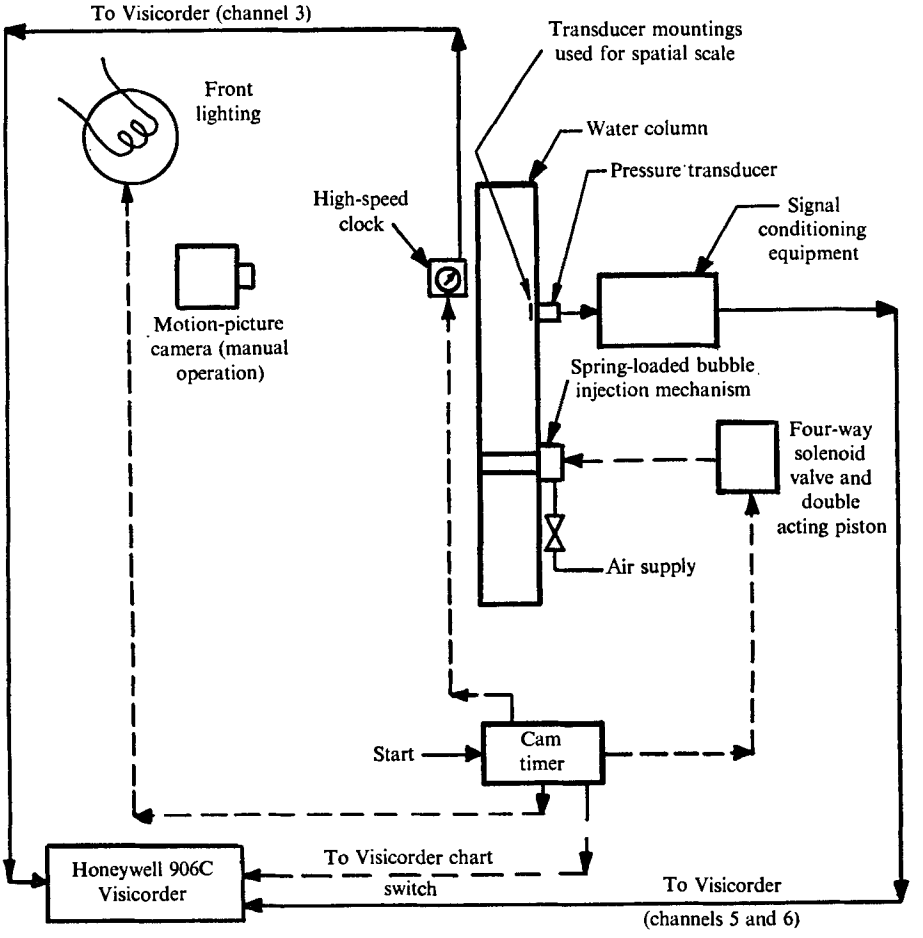

FIGURE 1. Schematic diagram of the experimental apparatus.

terminal velocity. The validity of the model is evaluated by comparison with selected pressure-field data. The pressure measurements also give information regarding the boundary and character of the bubble wake.

2. Description of the experiment

A single bubble is injected into a 'two-dimensional' water column, 36 in. wide, 69 in. high and $\frac{1}{2}$ in. thick, through a specially designed bubble injection mechanism. As the bubble rises, motion pictures and pressure measurements are taken simultaneously. A schematic diagram of the apparatus employed is shown in figure 1.

The water column was constructed from parallel plates spaced $\frac{1}{2}$ in. apart and both column walls were reinforced laterally to limit the maximum hydrostatic deflexion to 0·008 in. The bubble injection mechanism used was conceptually similar to that employed by Walters & Davidson (1961) and consisted of a

movable brass tube mounted in the rear wall of the column. The tube was filled with air and rapidly retracted to release a nearly circular bubble.

The pressure field resulting from the passage of the bubble through the water was measured by DISA 51F32 pressure transducers flush mounted in the rear wall of the column and recorded on a 906C Visicorder. Motion pictures of the bubble's rise were taken at a nominal speed of 200 frames/s with a 16 mm Hycam camera. Synchronization of the bubble's position with the recorded pressure–time traces was accomplished by including a high-speed clock in the camera's field of view and recording the instant at which the clock started.

A cam timer sequenced events of an experimental run automatically. Details of the equipment are given in Lazarek (1972).

3. Experimental data

Simultaneous pressure-field and photographic data were obtained for two bubble sizes ($1\frac{1}{2}$ and 2 in. initial diameter) and several transducer locations.

Bubble size, shape and rise velocity

Average values of the bubble width, height, aspect ratio, frontal radius and rise velocity computed from the motion pictures are presented in table 1. Also included in the table are standard deviations for the averaged bubble parameters. As seen there, the bubble's size, shape and rise velocity are extremely reproducible for both bubble diameters used in the experiment. The data for the rise velocity and aspect ratio are in good agreement with similar results in the literature (Collins 1965*b*, *c*; Pyle 1965; Maneri 1970). Details of this comparison are given in Lazarek (1972).

Pressure–time traces

The pressure–time traces for each experimental run were synchronized with the motion pictures and reduced to dimensionless form. The dimensionless variables consist of the pressure coefficient, a normalized time and a normalized lateral displacement.

The pressure coefficient C_p is defined as

$$C_p \equiv (p - p_\infty)/\tfrac{1}{2}\rho U^2, \tag{3.1}$$

where p_∞ is the static elevation head above a transducer at a given location, p is the pressure measured at that transducer location, U is the bubble rise velocity and ρ is the liquid density.

The normalized time Ut/a represents the distance travelled by the bubble in terms of the number of bubble half-widths. Ut/a is defined as zero when the bubble nose is at the same vertical height in the column as the transducer. With this definition Ut/a is negative when the transducer is located above the bubble nose and vice versa (see figure 2).

The normalized lateral displacement y/a represents the horizontal distance between the bubble's axis of symmetry ($y = 0$) and the vertical centre-line of the transducer.

Parameter	Initial bubble diameter = 2 in. Average value (61 runs)	Standard deviation	Initial bubble diameter = 1½ in. Average value (49 runs)	Standard deviation
Bubble width, $2a$ (in.)	4·62	0·0578	3·45	0·0518
Bubble height, h (in.)	1·05	0·0228	0·76	0·0163
Aspect ratio, h/a	0·46	0·0134	0·44	0·0115
Frontal radius of curvature, R† (in.)	3·55	0·0653	2·82	0·0779
Rise velocity, U (in./s.)	20·70	0·354	18·36	0·344

† Measured over 75° included angle.

TABLE 1. Data for bubble size, shape and rise velocity

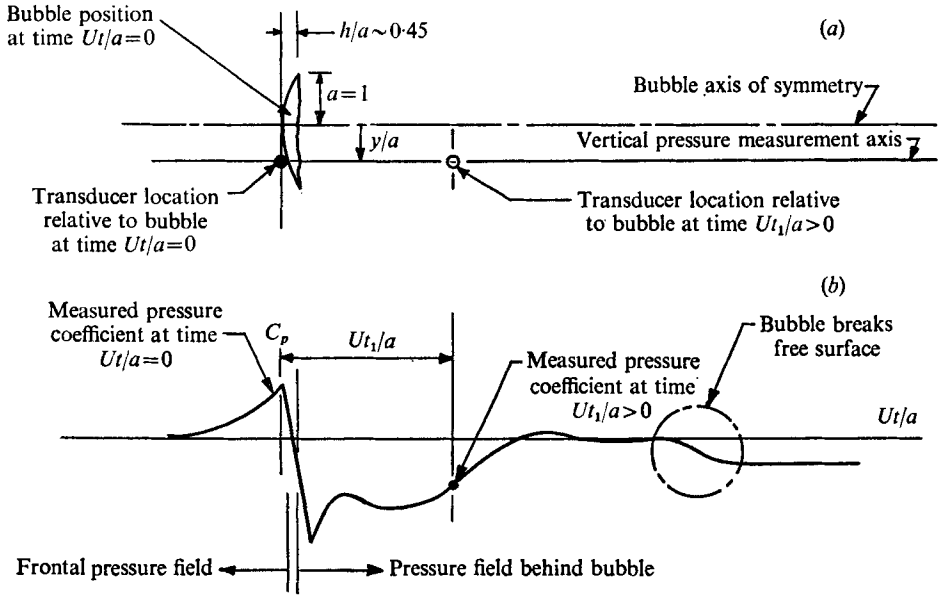

FIGURE 2. Bubble position relative to dimensionless pressure–time plots.

The location of the bubble relative to the transducer and the pressure measured by the transducer illustrate graphically the synchronization of the pressure–time curve (figure 2*b*) and the motion picture (figure 2*a*). Selected plots of C_p *vs.* Ut/a for various values of y/a are presented in figures 3–5 for the 2 in. bubbles used in the experiment. Additional data for the 1½ in. diameter bubbles given in Lazarek (1972) show similar trends.

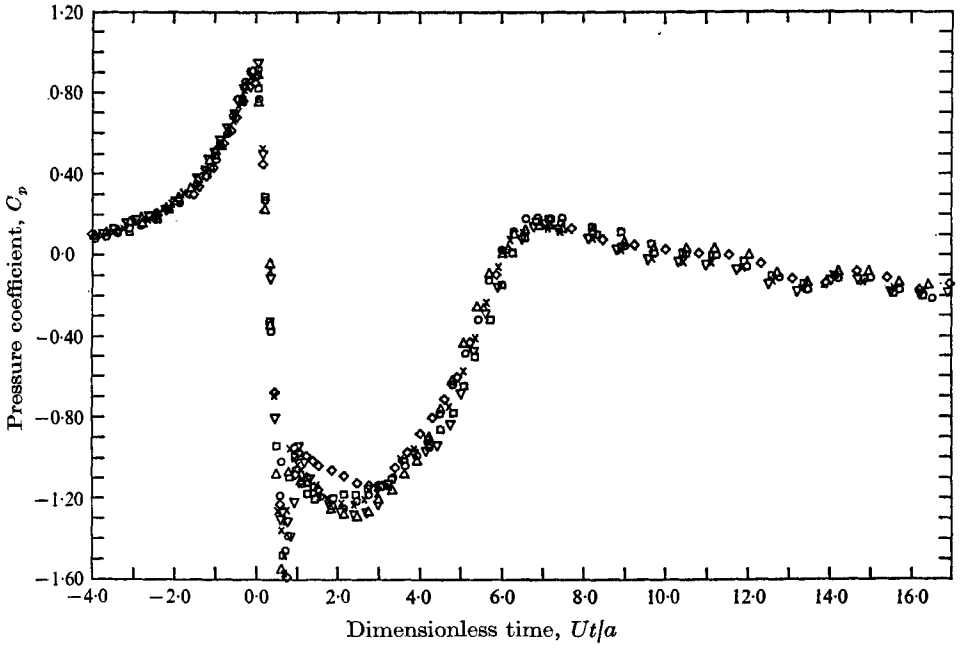

FIGURE 3. Axial pressure distribution along $y/a \sim 0$ for bubbles of initial diameter 2 in.

	□	○	△	▽	◇	×
Run	300–13	300–14	300–15	300–17	300–21	300–23
y/a	−0·13	0·00	−0·14	−0·03	−0·10	−0·07

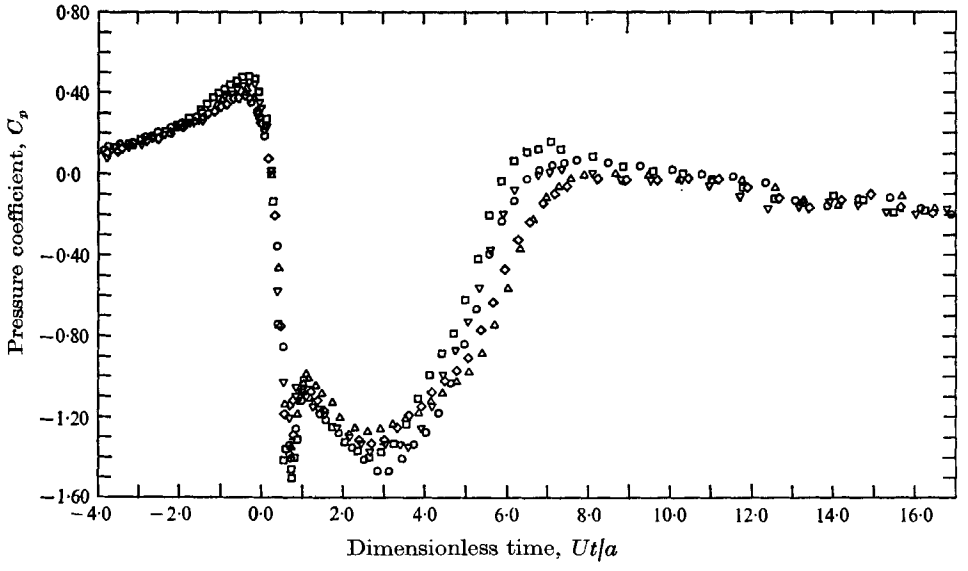

FIGURE 4. Axial pressure distribution along $y/a \sim 0{\cdot}85$ for bubbles of initial diameter 2 in.

	○	□	△	▽	◇
Run	300–01	300–07	300–08	300–10	300–12
y/a	0·97	0·75	0·86	0·82	0·90

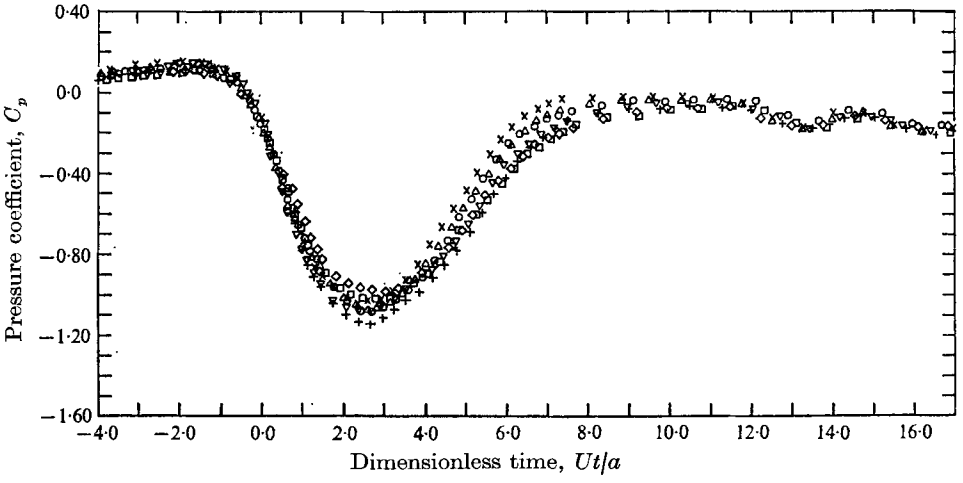

FIGURE 5. Axial pressure distribution along $y/a \sim -1{\cdot}80$ for bubbles of initial diameter 2 in.

	○	□	△	▽	◇	×	+
Run	300–25	300–26	300–28	300–29	300–31	300–34	300–35
y/a	−1·86	−1·82	−1·84	−1·70	−1·93	−1·83	−1·72

4. Analysis and discussion of the data

The dimensionless pressure-field plots are divided into three regions for purposes of discussion and analysis. These regions consist of (*a*) the frontal pressure field, (*b*) the pressure field between the bubble cap and floor and (*c*) the pressure field behind the bubble.

The frontal pressure field

In the region ahead of the bubble cap, the pressure-coefficient data are extremely reproducible and can be predicted from the two-dimensional model shown in figure 6. This model approximates the actual flow in front of a circular capped bubble by irrotational flow around an oval body. The front part of the oval corresponds to the bubble cap while the remaining portion of the oval provides a first approximation to the streamlines that leave the bubble rim and form the boundaries of the bubble wake.

The oval is constructed mathematically by combining the complex potentials for a source and sink of equal strength with that of a uniform stream. Effects due to the finite distance between the bounding walls are accounted for by an infinite reflexion of the source and sink according to the method of images.

There are two constants in the analytical model, which arise from the initially unspecified source–sink strength and from the source–sink spacing. A relation between the two constants is determined in the analysis by requiring the oval to pass through the bubble rim and the front stagnation point. This procedure ensures that the oval has a frontal geometry close to the circular cap shape observed experimentally. The remaining constant, the ratio of the source–sink spacing to the length of the oval, is bounded between zero and unity by physical

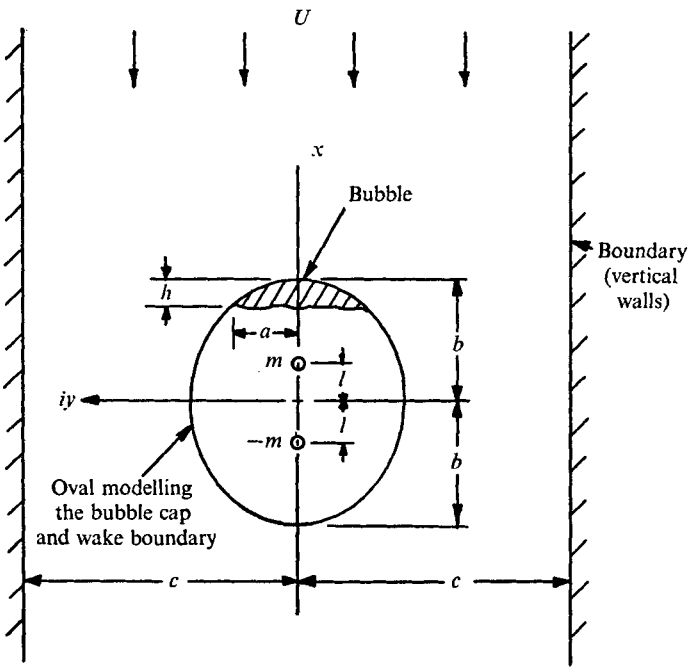

FIGURE 6. Analytical model for the frontal flow field.

considerations. By varying its magnitude, a variety of wake boundary modelling assumptions may be investigated. This feature of the model is important since the actual boundary of the wake is not known *a priori*, and a reasonable approximation to the true wake can be determined semi-empirically by comparing the model's predictions with data for the frontal pressure field.

The expression for the complex potential in dimensionless form is

$$\frac{W(z)}{Ua} = \frac{z}{a} - \frac{2}{\pi\mu}\frac{\sinh\left[\frac{1}{2}\pi\kappa\mu(1+\epsilon)\right]\sinh\left[\frac{1}{2}\pi\kappa\mu(1-\epsilon)\right]}{\sinh\pi\kappa\mu\epsilon}\ln\left[\frac{\sinh\frac{1}{2}\pi\mu(z/a-\epsilon\kappa)}{\sinh\frac{1}{2}\pi\mu(z/a+\epsilon\kappa)}\right], \quad (4.1)$$

where $$\epsilon = l/b, \quad \mu = h/a, \quad \kappa = b/a.$$

The relationship between ϵ and κ is obtained from the above-mentioned 'fitting' procedure by computing from (4.1) the oval streamline which passes through the points $(b, i0)$ and $(b-h, ia)$. This technique yields the following transcendental relation:

$$F(\kappa,\epsilon) \equiv \cosh\left[\pi\mu(\kappa-\nu)\right] - \cos(\pi\mu)\cosh(\pi\mu\epsilon\kappa)$$
$$-\sin(\pi\mu)\sinh(\pi\mu\epsilon\kappa)\cot\left\{\frac{(\pi\mu)\sinh(\pi\mu\epsilon\kappa)}{2\sinh\left[\frac{1}{2}\pi\kappa\mu(1+\epsilon)\right]\sinh\left[\frac{1}{2}\pi\kappa\mu(1-\epsilon)\right]}\right\} = 0, \quad (4.2)$$

where $$\nu = h/a.$$

In the remainder of the analysis, κ is considered fixed by (4.2) and ϵ is regarded as a parameter. The solution of (4.2) for values of ϵ between zero and unity has been obtained by Lazarek (1972) for the conditions used in the experiment.

The dynamic pressure coefficient, obtained in the usual way, is

$$C_p = 2G(\kappa,\mu,\epsilon)\,E\left(\frac{x'}{a},\frac{y}{a},\kappa,\mu,\epsilon\right) - G^2(\kappa,\mu,\epsilon)\left[E^2\left(\frac{x'}{a},\frac{y}{a},\kappa,\mu,\epsilon\right)+H^2\left(\frac{x'}{a},\frac{y}{a},\kappa,\mu,\epsilon\right)\right], \tag{4.3}$$

where

$$G(\kappa,\mu,\epsilon) = \frac{\sinh\left[\frac{1}{2}\pi\kappa\mu(1+\epsilon)\right]\sinh\left[\frac{1}{2}\pi\kappa\mu(1-\epsilon)\right]}{\sinh\pi\kappa\mu\epsilon}, \tag{4.4a}$$

$$x'/a = x/a-\kappa, \tag{4.4b}$$

$$E\left(\frac{x'}{a},\frac{y}{a},\kappa,\mu,\epsilon\right) = \frac{\sinh\pi\mu[x'/a+\kappa(1-\epsilon)]}{\cosh\pi\mu[x'/a+\kappa(1-\epsilon)]-\cos(\pi\mu y/a)} - \frac{\sinh\pi\mu[x'/a+\kappa(1+\epsilon)]}{\cosh\pi\mu[x'/a+\kappa(1+\epsilon)]-\cos(\pi\mu y/a)}, \tag{4.4c}$$

$$H\left(\frac{x'}{a},\frac{y}{a},\kappa,\mu,\epsilon\right) = \frac{\sin(\pi\mu y/a)}{\cosh\pi\mu[x'/a+\kappa(1-\epsilon)]-\cos(\pi\mu y/a)} - \frac{\sin(\pi\mu y/a)}{\cosh\pi\mu[x'/a+\kappa(1+\epsilon)]-\cos(\pi\mu y/a)}. \tag{4.4d}$$

Figures 7 (*a*)–(*d*) present a comparison between the analytical model and selected data for the frontal pressure field. The value 0·60 used for ϵ in the comparison was determined by superimposing theoretical results for different values of ϵ upon data plots similar to those presented in the figures. The superposition showed that reasonable agreement could be achieved for values of ϵ between 0·50 and 0·80. The value 0·60 was judged to give the 'best fit' to the data on an overall basis.

These figures show that there is a good measure of agreement between the theoretical model and the experimental data. The theory correctly predicts all the trends shown by the data: (i) a monotonically decreasing pressure coefficient along the vertical axis of symmetry above the stagnation point (figure 7*a*); (ii) the appearance of a pressure peak in front of the bubble at intermediate lateral displacements off the axis of symmetry (figure 7*b*) and (iii) a monotonic increase in pressure at large lateral displacements (figure 7*d*).

Quantitative agreement between the theory and the data is good. The difference between the predicted and the measured pressure coefficients is of the order of 0·05–0·10C_p except at a lateral displacement of $y/a = 2{\cdot}35$ (figure 7*c*), where x'/a is between $-0{\cdot}45$ and 0. In this region the theory differs from the data by about 0·15C_p. Although better agreement can be obtained there (figure 7*c*) by using $\epsilon = 0{\cdot}80$ (Lazarek 1972) it is important to recognize that ϵ can only have one value within the constraints of the analytical model.

Several oval shapes were computed as a function of ϵ and compared with a photograph of the wake given by Collins (1965*a*). As shown in figure 8, the oval shape with $\epsilon = 0{\cdot}5$ closely approximates the wake boundary observed by Collins and this value of ϵ is in reasonable agreement with the value 0·6 required to fit the data for the frontal pressure field.

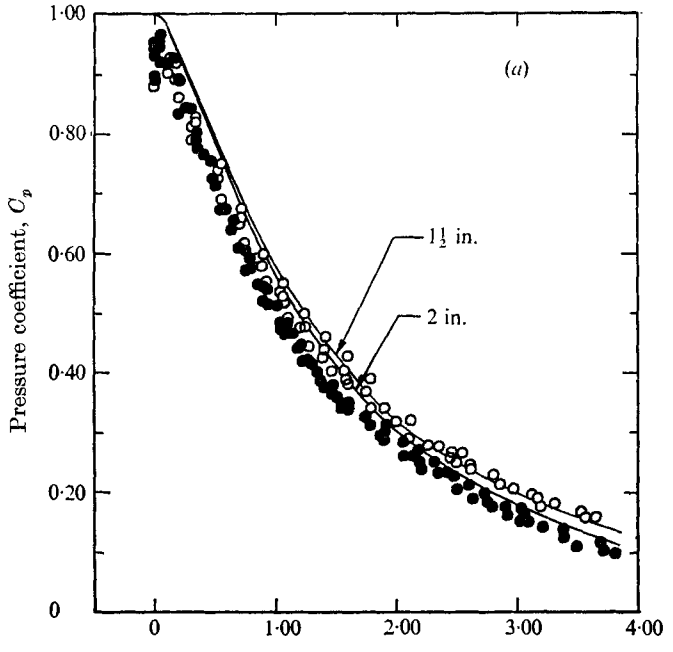

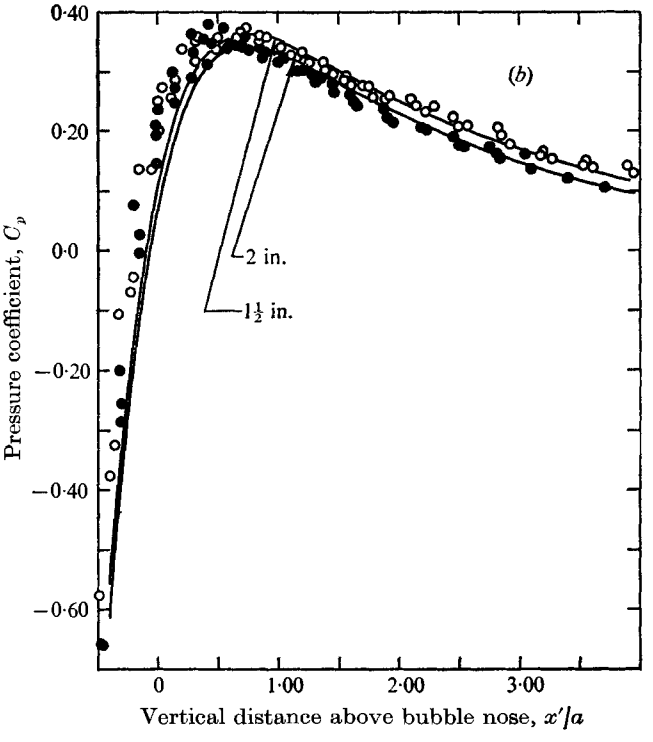

FIGURES 7(*a*, *b*). For legend see next page.

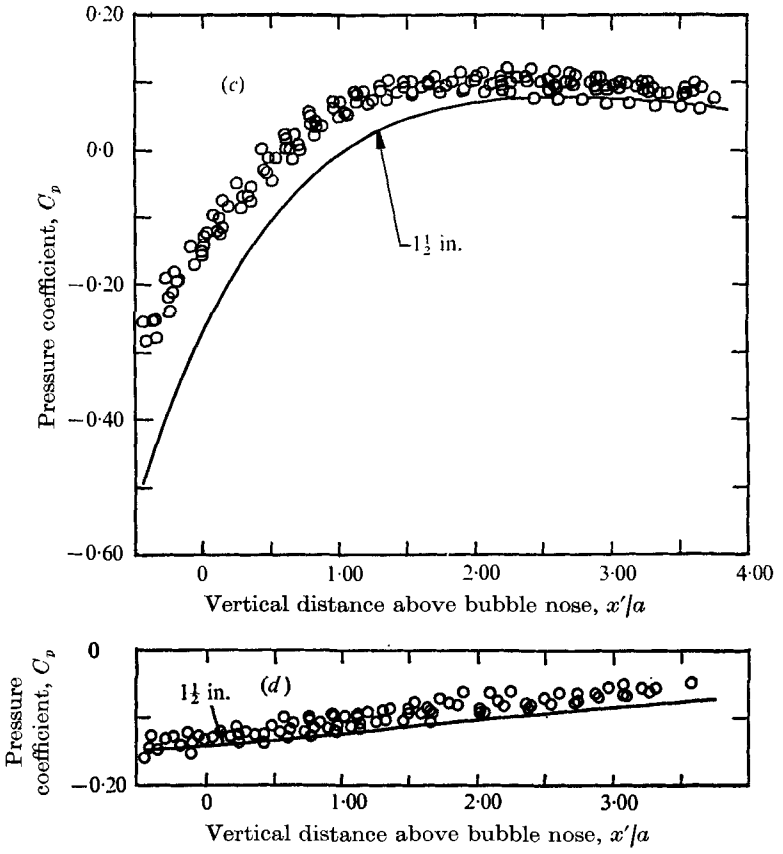

FIGURE 7. Comparison between the theoretical model and data for the frontal pressure field at a lateral displacement of (*a*) $y/a \sim 0$, (*b*) $y/a \sim 1{\cdot}00$, (*c*) $y/a \sim 2{\cdot}35$, (*d*) $y/a \sim 8{\cdot}75$. Bubble data: ●, initial diameter 2 in.; ○, initial diameter 1½ in. The curves marked 2 in. and 1½ in. are equation (4.3) with $\epsilon = 0{\cdot}60$ for bubbles of initial diameter 2 in. and 1½ in. respectively.

The pressure field between the bubble cap and the floor

In this region the pressure coefficient decreases linearly with increasing distance below the bubble nose (figures 3 and 4). As expected, the pressure within the region is quite uniform at a given instant of time. The theoretical expression for the pressure coefficient along the bubble cap is easily derived by the method of Davies & Taylor (1950):

$$C_p = 1 - 2gx/U^2, \tag{4.5}$$

where x is the vertical distance beneath the bubble nose.

Figure 9 compares the measured pressure coefficients with that predicted by (4.5). The theoretical cap pressure distribution agrees well with the experimental data for both bubble sizes used in the experiment. Admittedly, the data exhibit some scatter because of large axial pressure gradients that make measurements difficult in the vicinity of the bubble cap. However, the data are reproducible and show good quantitative agreement with the theory. These results experimentally verify the Davies & Taylor (1950) cap boundary condition.

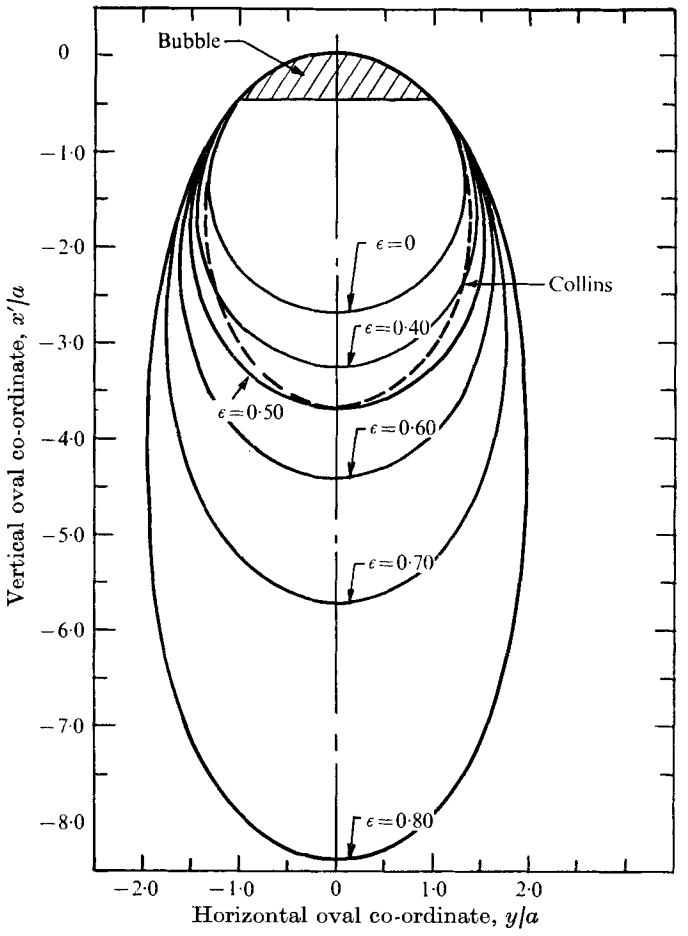

FIGURE 8. Shape of oval as a function of ϵ. $\nu = 0{\cdot}45$, $a = 1{\cdot}725$ in., $c = 18{\cdot}0$ in.

The pressure field behind the bubble

The data describing the third portion of the pressure field indicate that the axial pressure field extends as far as ten bubble half-widths below the bubble floor. Laterally, the dynamic pressure extends across approximately the full width of the water column, or about ten bubble half-widths from the bubble's vertical axis of symmetry for the $1\frac{1}{2}$ in. bubbles.

Different trends, dependent upon the lateral and axial displacements y/a and Ut/a, are observable from the pressure-coefficient data beneath the bubble. The pressure directly beneath the bubble is constant for about two-thirds of a bubble height. This is illustrated in figures 3 and 4 by the linear portion of the pressure–time curve between the bubble floor ($Ut/a \sim 0{\cdot}45$) and $Ut/a \sim 0{\cdot}75$. At $Ut/a \sim 0{\cdot}75$, the pressure coefficient reaches a minimum of about $-1{\cdot}50$. The data show that the linearity in the pressure–time curve extends laterally about 1·2 bubble half-widths on either side of the bubble's axis of symmetry. The behaviour of the pressure–time data in this region is probably due to a turbulent region of liquid that travels with the bubble.

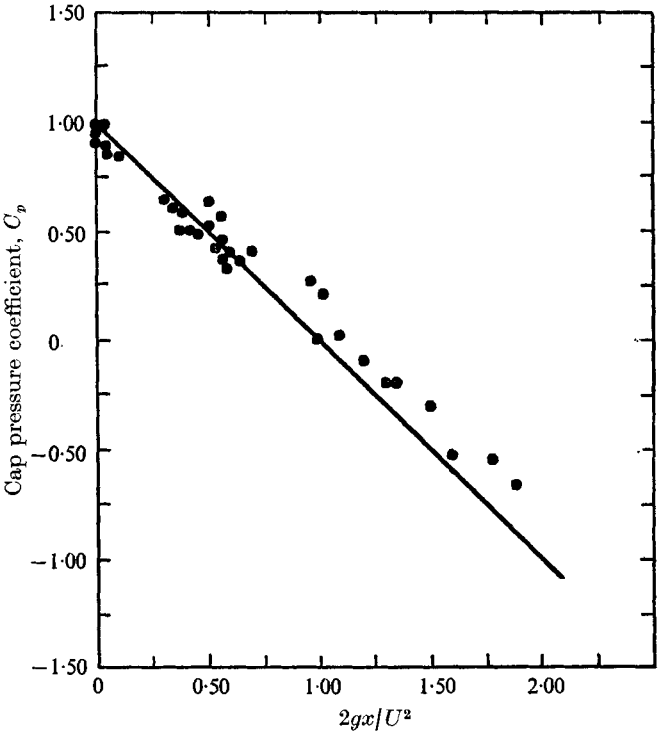

FIGURE 9. Theoretical and experimental pressure distributions along the bubble cap. ——, $C_p = 1 - 2gx/U^2$.

For lateral displacements less than $1{\cdot}20a$, the linear decrease in pressure below the bubble floor is followed by a sharp rise in pressure which is complete at a distance of about one bubble half-width ($Ut/a \sim 1{\cdot}0$). From this point, a gradual decrease in the pressure coefficient occurs up to a distance of three bubble half-widths ($Ut/a \sim 3{\cdot}0$). Then pressure recovery takes place up to $Ut/a \sim 7$. A slight 'overshoot' in pressure is observed at the end of the recovery region for lateral displacements less than one bubble half-width and the pressure coefficient remains positive from there on for a distance of about four bubble half-widths. The magnitude of the 'overshoot' varies somewhat with lateral displacement, having a pressure coefficient of about 0·10 near $y/a = 0$ and 0·0 near $y/a = 1$. After the 'overshoot' is complete, the pressure coefficient becomes flat with a magnitude near zero and remains so until the bubble breaks the free surface ($Ut/a \sim 12$). After this, the measured pressure coefficients oscillate slightly about a mean value corresponding to the change in water level caused by the lost bubble volume. The oscillatory pressure is associated with the settling motion of the free surface.

An additional investigation was performed to determine whether the overshoot was characteristic of the bubble wake or whether it was caused by bubble interaction with the free surface. Several runs were performed using bubbles of initial diameter 2 in. with a 40% reduction in the water level above the pressure transducers. Selected results of the study are presented in Lazarek (1972) and show

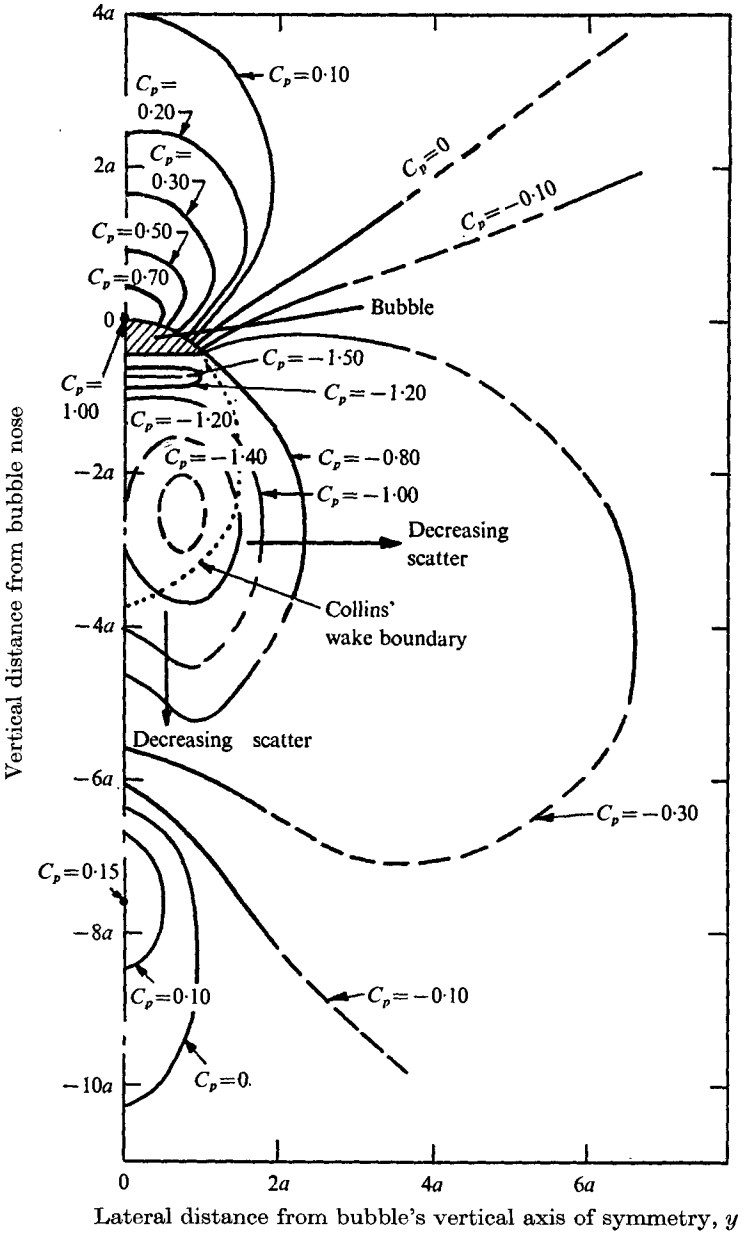

FIGURE 10. Isobaric representation of the pressure field for a bubble of initial diameter 2 in.

that the 'overshoot' characteristic of the pressure field beneath the bubble is due to the bubble wake and not to interactions between the bubble and the free surface.

The pressure-field data beneath the bubble may be interpreted with respect to the visual wake studies of Collins (1965*c*) and also Crabtree & Bridgwater (1967). For this purpose, an isobaric representation of the pressure field was

constructed for a bubble of initial diameter 2 in. by cross-plotting the dimensionless pressure–time traces. Figure 10 presents the resultant isobaric plot, where lines of constant pressure coefficient are shown relative to a stationary bubble. Portions of the isobars where some uncertainty exists, owing to either a scarcity of data or scatter in the data, are shown by dashed lines.

The wake boundary observed by Collins for a circular capped bubble at a Reynolds number similar to that used in the present study ($\sim 2 \times 10^4$) is also shown in figure 10. Collins found a closed wake structure consisting of a trailing vortex pair inside an elliptical or oval boundary. A 'smoother' type of flow characterized by more gradual streamlines was observed to exist outside that region. Three characteristics of the pressure-field data support the contention that a wake structure similar to that observed by Collins was also encountered in the present experiments.

(i) Symmetry of the pressure field about the bubble's vertical axis.

(ii) The scatter in the pressure-field data is largest in a region extending 1·5 bubble half-widths from the axis of symmetry and downward for about 4 bubble half-widths beneath the bubble nose (see figure 10). Outside this region, which corresponds approximately to Collins' wake, the scatter in the pressure-field data decreases rapidly in the lateral direction, indicating transition there to a well-ordered flow field.

(iii) Pressure minima are observed at $y/a = \pm 0{\cdot}75$, $Ut/a = 2{\cdot}5$, and are inside Collins' wake boundary and close to his vortex centres.

Further evidence for an elliptical or oval wake is provided by the analysis of the frontal pressure field, which indicates that the frontal pressure field is strongly influenced by the boundaries of the wake. Good agreement between the theoretical analysis and the pressure-distribution data was obtained when the wake boundary was allowed to take on an oval form. Relatively poor agreement with the data occurs when the wake boundary either degenerates to that of a cylinder or has an extremely large axial length, somewhat typical of the infinite wake models used in past analyses of rise velocity (Collins 1967; Rippin & Davidson 1967).

Our experimental pressure-field results do not agree with the wake studies of Crabtree & Bridgwater. They found the bubble wake to be characterized by an alternate vortex shedding process at Reynolds numbers similar to those encountered in this investigation. If alternate vortex shedding had occurred in the present study, vortices would be staggered behind the bubble and travel upwards at a velocity less than the bubble rise velocity. Depending upon the translational velocity of the vortex centres, a variety of pressure distributions could be measured at a fixed point in space. All, however, would exhibit a large asymmetry in the lateral direction owing to staggering of the vortices. Such a trend is not indicated by the pressure-field data.

Further indication that the wake was of a non-shedding type is provided by the high-speed motion pictures taken for each experimental run. These data show that the circular capped bubbles used in the experiment rose on rectilinear paths with little or no lateral motion. If vortex shedding had occurred, the bubbles would not have risen rectilinearly. Instead a rocking type of motion would have

been observed each time a vortex was discharged from the bubble rim (Lindt 1971). It is likely that the form of the wake observed by Crabtree & Bridgwater was related to their dump cup method of producing the bubble.

The Reynolds numbers that characterize the bubble rise are reasonably high, so that turbulence, as well as the diffusion of vorticity, probably controls the momentum distribution and energy dissipation in the wake. Additional research is necessary to understand these effects and to develop a quantitative description of the wake.

The authors are grateful to the Atomic Energy Commission for partial support of this work under Grant AT(30-1)-3639.

REFERENCES

COLLINS, R. 1965*a* *J. Fluid Mech.* **25**, 469.
COLLINS, R. 1965*b* *J. Fluid Mech.* **22**, 763.
COLLINS, R. 1965*c* *Chem. Engng Sci.* **20**, 851.
COLLINS, R. 1967 *Chem. Engng Sci.* **22**, 89.
CRABTREE, J. R. & BRIDGWATER, J. 1967 *Chem. Engng Sci.* **22**, 1517.
DAVIES, R. M. & TAYLOR, G. I. 1950 *Proc. Roy. Soc.* A **200**, 375.
GRACE, J. R. & HARRISON, D. 1967 *Chem. Engng Sci.* **22**, 1337.
HABERMAN, W. L. & MORTON, R. K. 1953 *David Taylor Model Basin Rep.* NR-715-102.
LAZAREK, G. M. 1972 Ph.D. thesis, Rensselaer Polytechnic Institute.
LINDT, J. T. 1971 *Chem. Engng Sci.* **26**, 1776.
MANERI, C. C. 1970 Ph.D. thesis, Polytechnic Institute of Brooklyn.
MANERI, C. C. & MENDELSON, H. D. 1968 *A.I.Ch.E. J.* **14**, 295.
MAXWORTHY, T. 1967 *J. Fluid Mech.* **27**, 367.
MENDELSON, H. D. 1967 *A.I.Ch.E. J.* **13**, 250.
PYLE, D. L. 1965 Ph.D. thesis, Cambridge University.
RIPPIN, D. W. T. & DAVIDSON, J. F. 1967 *Chem. Engng Sci.* **22**, 217.
ROSENBERG, B. 1950 *David Taylor Model Basin Rep.* no. 727.
WALTERS, J. K. & DAVIDSON, J. F. 1961 *J. Fluid Mech.* **12**, 408.